Electron–Phonon Scattering in Metallic Single-Walled Carbon Nanotubes

Ji-Yong Park, Sami Rosenblatt, Yuval Yaish, Vera Sazonova, Hande Üstünel, Stephan Braig, T. A. Arias, Piet W. Brouwer, and Paul L. McEuen*

Laboratory of Atomic and Solid-State Physics, Cornell University, Ithaca, New York 14853

Received December 31, 2003

ABSTRACT

Electron scattering rates in metallic single-walled carbon nanotubes are studied using an atomic force microscope as an electrical probe. From the scaling of the resistance of the same nanotube with length in the low- and high-bias regimes, the mean-free paths for both regimes are inferred. The observed scattering rates are consistent with calculations for acoustic-phonon scattering at low biases and zone boundary/optical phonon scattering at high biases.

Phonons in carbon nanotubes (NTs) has been an active area of research in recent years.[1] The effects of phonons have been measured in thermal transport,[2–4] Raman scattering,[1] and electrical transport.[5–7] Electron−phonon coupling in NTs is predicted to lead to a Peierls instability[8–11] and superconductivity[12,13] and contributes to the thermopower[14] and the resistivity[5,15–17] of NTs. At room temperature, the main origin of the resistivity at low bias in high-quality metallic single-walled nanotubes (SWNTs) is believed to be scattering by acoustic phonons.[5] The scattering is weak, resulting in long mean-free paths at room temperature. Both measurements and calculations put the mean-free path in the range of a few hundred nanometers to several micrometers.[5,6,15,17–19] At high biases, electrons gain enough energy to emit optical or zone-boundary phonons. Yao et al. showed that this scattering is very effective, leading to a saturation of the current at ~ 20 μA[7] at high biases. This work indicated that the fundamental high-energy phonon scattering rate was rapid but did not determine its value.

In this letter, we study electron−phonon scattering in metallic SWNTs in both the low- and high-bias regimes. We investigate the scaling of the resistance in a single NT for lengths ranging from 50 nm to 10 μm by using the tip of an atomic force microscope (AFM) as a movable electrode. For low biases, we find a length-independent resistance for $L < 200$ nm, indicating ballistic transport in the NT. At longer lengths, the scaling of the resistance with length is used to infer a low-bias mean-free path of $l_{low} \approx 1.6$ μm, consistent with previous measurements and calculations. For high biases and long channel lengths, the current saturates as in the previous study.[7] However, for short channel lengths $L < 500$ nm, the current does not saturate but rather grows linearly

with increasing bias. From measurements at different lengths, we infer that the high-bias mean-free path $l_{high} \approx 10$ nm is more than 100 times shorter than l_{low}. We present calculations of the electron−phonon scattering rate due to acoustic phonons, relevant for low biases, and optic and zone-boundary phonon emission, relevant at high biases. We obtain good agreement with our experimental results in both cases.

The SWNTs used in this study were grown by chemical vapor deposition at lithographically defined catalyst sites on a degenerately doped Si substrate with a 200-nm-thick oxide.[20,21] Metal electrodes were formed on the NT by evaporating 50-nm Au with a 5-nm Cr adhesion layer or 30-nm Au without an adhesion layer, followed by liftoff. Devices with direct Au contacts show better contact resistances after initial fabrication. Devices with Cr/Au contacts were annealed at ~ 600 °C after the fabrication to enhance the NT−metal contact. All of the measurements reported here were performed on metallic SWNTs, as determined by the gate-voltage dependence of the conductance and a saturation current of 19−25 μA at high biases and long channel lengths.[22]

For this study, an AFM operating at ambient conditions with the capability of simultaneous transport measurements was used.[23] Figure 1 shows a schematic of the three-probe measurement geometry.[24] In addition to the two lithographic electrodes, an Au-coated AFM tip serves as a third electrode by making physical and electrical contact with the NT.[25,26] A bias voltage V_{sd} is applied to the source electrode (the left electrode in Figure 1), and the resulting current is measured by a current amplifier attached to the AFM tip, which serves as the drain electrode. This yields I as a function of V_{sd}. We also use the second lithographic contact (right electrode in
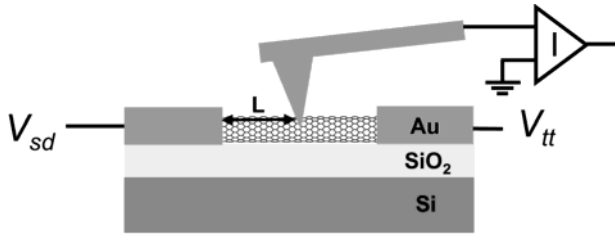
Figure 1. Schematic of the three-probe measurement setup. The two electrodes and the Au-coated AFM tip serve as a voltage source (left electrode), voltage probe (right electrode), and current probe (AFM tip), respectively. The active length L of the SWNT device can be changed by moving the AFM tip.
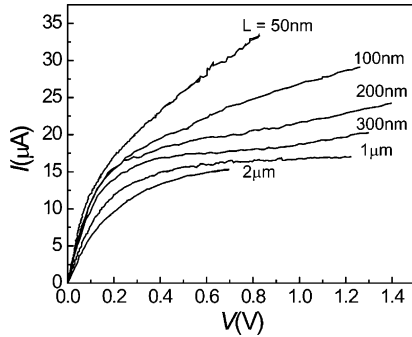

Figure 2. Current I versus voltage V at different lengths for an SWNT device of overall length 10 μm and tube diameter 1.8 nm. The measured length L of the tube is indicated next to each curve.

Figure 1) as a voltage probe to measure the voltage drop V_{tt} at the tip−tube drain junction. From this, we can deduce the voltage $V = V_{sd} - V_{tt}$ and hence the I−V curve that corresponds to just the left contact and the SWNT segment between this contact and the tip. By moving the tip to different locations along the tube, I−V measurements of the same SWNT for different channel lengths L are obtained.[27] Because the left contact is always the same and the voltage drop associated with the right AFM contact is subtracted, measurements at different channel lengths can be directly compared. The shortest channel length that we can measure in this way depends on the stability of the AFM and the size of the tip, but it is typically $L \approx 50$ nm.

Figure 2 is the result of measurements of I versus V on a 10-μm-long metallic SWNT at six different tip-contact

separations L. We first concentrate on the low-bias region where the I−V characteristic is linear. In Figure 3a, the low-bias resistance $R_{low} = \mathrm{d}V/\mathrm{d}I$ is plotted for each length. For L between 50 and 200 nm, R_{low} is almost constant, but it increases linearly with L for longer lengths. The slope of this line is the 1D resistivity $\rho = \mathrm{d}R_{low}/\mathrm{d}L \approx 4$ kΩ/μm. Similar resistivity is found for several other metallic SWNTs.

The resistivity of a 1D channel with four subbands in the incoherent limit is given by[28]

$$\rho = \left(\frac{h}{4e^2}\right)\left(\frac{1}{l}\right) \qquad (1)$$

where l is the electron mean-free path for backscattering. From the measured slope, we infer that $l_{low} \approx 1.6$ μm. For measurements with $L \ll l_{low}$, the transport is essentially ballistic. The measured resistance is just the contact resistance associated with the source contact and is constant.

Now we consider the high-bias regime. The slope of the I−V curve decreases with increasing V. For long channel lengths, the current saturates to an approximately constant value of ∼20 μA as reported previously.[7] For shorter lengths $L < 500$ nm, however, different behavior is observed. The current again increases linearly with V at high bias but with a slope much lower than at low bias.

The inverse slopes of I−V curves at high bias, $R_{high} = \mathrm{d}V/\mathrm{d}I$, from four devices with diameters in the range of 1.8 < d/nm < 2.5 are shown in Figure 3b. R_{high} scales linearly with L, with a slope of $\mathrm{d}R_{high}/\mathrm{d}L = 800$ kΩ/μm. This high-bias resistivity is 200 times larger than at low bias. If we use eq 1 to infer a mean-free path, then we obtain $l_{high} \approx 10$ nm.

We now compare these results to expectations for electron−phonon scattering in NTs. The electron−phonon coupling is described by the Hamiltonian

$$H_{ep} = \sum_{\mathbf{k},\mathbf{q}} D_{\mathbf{k},\mathbf{q}}^{\alpha} c_{\mathbf{k}+\mathbf{q}}^{\dagger} c_{\mathbf{k}} u_{\mathbf{q}}^{\alpha} \qquad (2)$$

$$u_{\mathbf{q}}^{\alpha} = \sqrt{\frac{\hbar}{2L\rho\Omega_{\mathbf{q}}^{\alpha}}}(b_{\mathbf{q}}^{\alpha} + b_{-\mathbf{q}}^{\alpha\dagger})$$

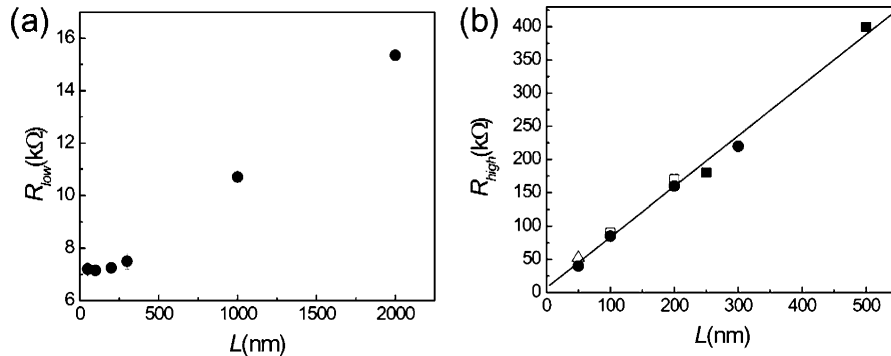where $\mathbf{q}$ and α label the phonon wavevector and branch,

Figure 3. (a) Low-bias resistance $R_{low} = \mathrm{d}V/\mathrm{d}I$ near zero bias as a function of L for the SWNT in Figure 2. (b) High-bias resistance $R_{high} = \mathrm{d}V/\mathrm{d}I$ versus L from four different SWNTs. The diameters of the SWNTs are 1.8 nm (●, from the device in Figure 2), 2 nm (■, □), and 2.5 nm (△). The line is a linear fit to the data.
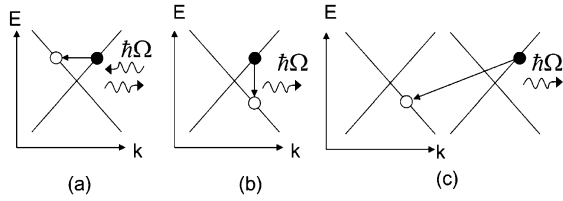
Figure 4. Diagrams showing electron−phonon scattering in a metallic SWNT by phonons with energy $\hbar\Omega$ that satisfies energy and momentum conservation. (a) Emission and absorption of an acoustic phonon with low energy and small momentum. (b) Emission of an optical phonon (high energy and small momentum) and (c) a zone-boundary phonon (high energy and large momentum).

respectively, u is the phonon displacement, $c^\dagger$ and c ($b^\dagger$ and b) are electron (phonon) creation and annihilation operators, respectively, L is the length of an NT, and ρ is the mass density. For application to electron transport, the electron wavevectors $\mathbf{k}$ and $\mathbf{k} + \mathbf{q}$ are taken in the vicinity of the Fermi points of the NT. The electron−phonon scattering of electrons from an initial state with wavevector $\mathbf{k}$ and energy $E_\mathbf{k}$ to a final state with wavevector $\mathbf{k} + \mathbf{q}$ and energy E_{k+q} must conserve energy,

$$E_{\mathbf{k}+\mathbf{q}} = E_\mathbf{k} \pm \hbar\Omega_\mathbf{q}^\alpha \qquad (3)$$

where the plus sign refers to the absorption of a phonon with wavevector $\mathbf{q}$ and the minus sign refers to the emission of a phonon with momentum $-\mathbf{q}$. Examples of scattering processes that meet these criteria in NT are shown schematically in Figure 4.

For acoustic phonons, one has $D_{\mathbf{k}_{F,\mathbf{q}}}^\alpha = \Xi^\alpha q$, where Ξ^α is the deformation potential. Using Fermi's golden rule along with a thermal occupation of phonon states ($\hbar\Omega_\mathbf{q}^\alpha \ll kT$ for acoustic phonons) and combining contributions from the emission and absorption of acoustic phonons, one arrives at the electron−acoustic-phonon scattering rate

$$\frac{1}{\tau_{ac}} = 2\frac{2\pi}{\hbar}\Xi^2\left(\frac{k_BT}{2\rho v_s^2}\right)\frac{1}{h v_F} \qquad (4)$$

where $v_s = \Omega_\mathbf{q}/q$ is the acoustic-phonon velocity. The maximum deformation potential for an acoustic phonon from a band gap change in metallic SWNTs with uniaxial or torsional strain is $\Xi \approx 5$ eV.[29] Then from eq 4, we compute the scattering time, $\tau_{ac} \approx 3.0 \times 10^{-12}$ s for an SWNT with a diameter of 1.8 nm and the corresponding mean-free path, $l_{ac} = v_F\tau_{ac} \approx 2.4$ μm. This calculated acoustic-phonon scattering rate is comparable to previous calculations.[5,15]

Because there are two possible origins of electron scattering at low bias—disorder and acoustic phonons—the experimentally measured value l_{low} is a lower limit for the acoustic-phonon scattering mean-free path: $l_{low} < l_{ac}$. The data are therefore consistent with the theory. These measurements confirm the weak electron−acoustic-phonon scattering and long mean-free path values previously reported in SWNTs.[5,6,18,19]
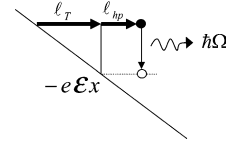
Figure 5. Schematic showing the two relevant length scales for high-bias electron−phonon scattering. The total scattering length is the sum of l_T, the distance electron must accelerate in the electric field ϵ to reach a threshold energy $\hbar\Omega$, and l_{hp}, the high-energy phonon scattering mean-free path.

We now turn to the case of optical and zone-boundary phonons, where the scattering length has not been determined previously. Because no such phonons are present at room temperature ($\hbar\Omega \gg k_BT$), scattering from optical or zone-boundary phonons will involve emission only if we assume that any emitted phonons relax instantaneously. These processes are shown in Figure 4b and c. According to Fermi's golden rule, the scattering rate from spontaneous phonon emission is

$$\frac{1}{\tau_\mathbf{q}^\alpha} = \frac{2\pi}{\hbar}|D_\mathbf{k}^\alpha F_{,\mathbf{q}}|^2\left(\frac{\hbar}{2\rho\Omega_\mathbf{q}^\alpha}\right)\frac{1}{h v_F} \qquad (5)$$

Using a tight-binding model,[30] we calculated the relevant matrix elements $D_{\mathbf{k},\mathbf{q}}^\alpha$ in the electron−phonon Hamiltonian by considering the creation of a band gap in NT with respect to the atomic displacements corresponding to the phonon mode. For optical phonons ($\mathbf{q} = 0$), we found that only displacements compatible with the longitudinal mode lead to a band gap.[31] From this model, we obtain $D \approx 12.8$ eV/Å, corresponding to the scattering time $\tau_{op} \approx 2.3 \times 10^{-13}$ s and the mean-free path $l_{op} \approx 180$ nm. For the zone-boundary phonon ($\mathbf{q} = -2\mathbf{k}_F$), we found that only one optical mode gives a significant band gap and the contributions of other optical and acoustic modes are small. For this mode, we found $D \approx 25.6$ eV/Å, yielding $\tau_{zo} \approx 4.6 \times 10^{-14}$ s and $l_{zo} \approx 37$ nm. Unlike the acoustic scattering mean-free path, which depends on the type of nanotube, the mean-free paths l_{op} and l_{zo} do not depend on the type of NT as long as the NT is metallic.

In principle, to calculate the effect of high-energy scattering processes on the $I−V$ characteristics, the Boltzmann equation must be solved self-consistently to determine the occupancies of the initial and final states. In the limiting case of high bias, however, simple arguments can be given that are sufficient for an interpretation of the data.

Following ref 5, an electron must first accelerate a length l_T in the electric field ϵ to attain sufficient excess energy to emit an optical phonon ($\hbar\Omega \approx 0.2$ eV) or zone-boundary phonon ($\hbar\Omega \approx 0.16$ eV). This length is given by $l_T = \hbar\Omega/e\epsilon = (\hbar\Omega/\mathrm{eV})\cdot L$. Once it attains this energy, it will scatter on a length scale of the high-energy phonon scattering mean-free path (l_{hp}). The total length that the electron traverses before scattering is, therefore, on the order of $l_T + l_{hp}$, as illustrated in Figure 5.

For large enough L ($l_T \gg l_{hp}$), the scattering length will be determined by l_T. The high-bias resistance is then $R =$

$(h/4e^2)(L/l_T) + R_{low} = V/I_0 + R_{low}$, which implies a current saturation with $I_o = (4e/h)\hbar\Omega$.[7] This is valid for the longer channel lengths in Figure 2. However, if L is sufficiently small ($l_T \ll l_{hp}$), then the scattering length will be determined by l_{hp}. Then, the high-bias resistance is $R_{high} = (h/4e^2)(L/l_{hp}) + R_{low}$. In short channels, then, the measured scattering length should be l_{hp}.[32] Because both optical and zone-boundary phonons contribute, we can deduce the scattering length from our calculations by $l_{hp}^{-1} = l_{op}^{-1} + l_{zo}^{-1}$: $l_{hp} \approx 30$ nm.

This theoretical value is in reasonable agreement with the experimental finding: $l_{high} \approx 10$ nm. The difference could arise from uncertainties in the parameters of the theory or from additional scattering mechanisms not considered here. These include multiple phonon scattering or stimulated phonon emission from high-energy phonons created by other scattering events. The latter process will be important if the phonons cannot rapidly escape the NT into the substrate. Measurements at high bias on suspended NTs[33] should shed light on this issue.

In conclusion, we have investigated the scaling with channel length of the $I-V$ characteristics of metallic SWNTs. The mean-free paths for electron−acoustic-phonon scattering ($l_{ac} > 1.6\ \mu m$) and high-energy phonon scattering ($l_{high} \approx 10$ nm) at room temperature were measured and compared to theory. In addition to their fundamental interest, these results are important for uses of SWNTs in high-current applications such as interconnects or transistors operating in the saturation region. Our results show that the scattering length at high bias is more than 100 times shorter than at low bias. Nevertheless, in short devices, the current carried by an SWNT can significantly exceed the previously reported limit of 25 μA.[7]

Note Added in Proof: During the final preparation of this paper, we became aware of work by another group reaching similar conclusions.[35]

References

(1) Dresselhaus, M. S.; Eklund, P. C. *Adv. Phys.* **2000**, *49*, 705.
(2) Hone, J.; Whitney, M.; Piskoti, C.; Zettl, A. *Phys. Rev. B* **1999**, *59*, R2514.
(3) Kim, P.; Shi, L.; Majumdar, A.; McEuen, P. L. *Phys. Rev. Lett.* **2001**, *87*, 215502.
(4) Small, J. P.; Shi, L.; Kim, P. *Solid State Commun.* **2003**, *127*, 181.
(5) Kane, C. L.; Mele, E. J.; Lee, R. S.; Fischer, J. E.; Petit, P.; Dai, H.; Thess, A.; Smalley, R. E.; Verschueren, A. R. M.; Tans, S. J.; Dekker: C. *Europhys. Lett.* **1998**, *41*, 683.
(6) Appenzeller, J.; Martel, R.; Avouris, P.; Stahl, H.; Lengeler, B. *Appl. Phys. Lett.* **2001**, *78*, 3313.
(7) Yao, Z.; Kane, C. L.; Dekker, C. *Phys. Rev. Lett.* **2000**, *84*, 2941.
(8) Dubay, O.; Kresse, G.; Kuzmany, H. *Phys. Rev. Lett.* **2002**, *88*, 235506.
(9) Figge, M. T.; Mostovoy, M.; Knoester, J. *Phys. Rev. B* **2002**, *65*, 125416.
(10) Mintmire, J. W.; Dunlap, B. I.; White, C. T. *Phys. Rev. Lett.* **1992**, *68*, 631.
(11) Saito, R.; Fujita, M.; Dresselhaus, G.; Dresselhaus, M. S. *Phys. Rev. B* **1992**, *46*, 1804.
(12) Benedict, L. X.; Crespi, V. H.; Louie, S. G.; Cohen, M. L. *Phys. Rev. B* **1995**, *52*, 14935.
(13) De Martino, A.; Egger, R. *Phys. Rev. B* **2003**, *67*, 235418.
(14) Scarola, V. W.; Mahan, G. D. *Phys. Rev. B* **2002**, *66*, 205405.
(15) Jishi, R. A.; Dresselhaus, M. S.; Dresselhaus, G. *Phys. Rev. B* **1993**, *48*, 11385.
(16) Woods, L. M.; Mahan, G. D. *Phys. Rev. B* **2000**, *61*, 10651.
(17) Suzuura, H.; Ando, T. *Phys. Rev. B* **2002**, *65*, 235412.
(18) Hertel, T.; Fasel, R.; Moos, G. *Appl. Phys. A* **2002**, *75*, 449.
(19) Bachtold, A.; Fuhrer, M. S.; Plyasunov, S.; Forero, M.; Anderson, E. H.; Zettl, A.; McEuen, P. L. *Phys. Rev. Lett.* **2000**, *84*, 6082.
(20) Kong, J.; Soh, H. T.; Cassell, A. M.; Quate, C. F.; Dai, H. J. *Nature* **1998**, *395*, 878.
(21) Rosenblatt, S.; Yaish, Y.; Park, J.; Gore, J.; Sazonova, V.; McEuen, P. L. *Nano Lett.* **2002**, *2*, 869.
(22) See ref 7. Current saturation values significantly above 25 μA are seen for devices with more than one NT, multiwalled NTs, or a bundle of SWNTs.
(23) Park, J.-Y.; Yaish, Y.; Brink, M.; Rosenblatt, S.; McEuen, P. L. *Appl. Phys. Lett.* **2002**, *80*, 4446.
(24) Yaish, Y.; Park, J.-Y.; Rosenblatt, S.; Sazonova, V.; Brink, M.; McEuen, P. L. *Phys. Rev. Lett.* **2004**, *92*, 046401.
(25) de Pablo, P. J.; Gomez-Navarro, C.; Colchero, J.; Serena, P. A.; Gomez-Herrero, J.; Baro, A. M. *Phys. Rev. Lett.* **2002**, *88*, 036804.
(26) de Pablo, P. J.; Gomez-Navarro, C.; Martinez, M. T.; Benito, A. M.; Maser, W. K.; Colchero, J.; Gomez-Herrero, J.; Baro, A. M. *Appl. Phys. Lett.* **2002**, *80*, 1462.
(27) To exclude any possible effects due to damage introduced by the AFM tip, all of the measurements were made while approaching the source electrode, starting at the longest length.
(28) Datta, S. *Electronic Transport in Mesoscopic Systems*; Cambridge University Press: London, 1995.
(29) Yang, L.; Han, J. *Phys. Rev. Lett.* **2000**, *85*, 154.
(30) Goodwin, L. *J. Phys.: Condens. Matter* **1991**, *3*, 3869.
(31) Dubay, O.; Kresse, G. *Phys. Rev. B* **2003**, *67*, 035401.
(32) Another potential mechanism for increased current above the saturation limit is transport through noncrossing subbands and inter-subband Zener tunneling.[34] Because the first noncrossing subband in a 1−2-nm-diameter metallic SWNT is more than 1.5−3 eV above the Fermi level, this effect should be negligible.
(33) Tombler, T. W.; Zhou, C. W.; Alexseyev, L.; Kong, J.; Dai, H. J.; Lei, L.; Jayanthi, C. S.; Tang, M. J.; Wu, S. Y. *Nature* **2000**, *405*, 769.
(34) Anantram, M. P. *Phys. Rev. B* **2000**, *62*, R4837.
(35) Javey, A.; Guo, J.; Paulsson, M.; Wang, Q.; Mann, D.; Lundstrom, M.; Dai, H. cond-mat/0309242.

NL035258C